The influence of constitutive material models on accumulated plastic strain in finite element weld analyses

O. Muránsky [a,*], C.J. Hamelin [a], V.I. Patel [a,b], V. Luzin [c], C. Braham [d]

[a] ANSTO, Institute of Materials Engineering, New Illawarra Road, Lucas Heights, NSW, Australia
[b] UNSW, School of Civil and Environmental Engineering, Faculty of Engineering, Sydney, NSW, Australia
[c] ANSTO, Bragg Institute, New Illawarra Road, Lucas Heights, NSW, Australia
[d] Laboratoire de Procédés et Ingénierie en Mécanique et Matériaux (PIMM-UMR CNRS 8006), ENSAM, 151, Boulevard de l'Hôpital, 75013 Paris, France

Keywords:
Residual stresses
Plastic strain
Plasticity theory
Annealing
Finite element analysis

A B S T R A C T

Recent studies in computational weld mechanics have revealed the importance of the material plasticity model when predicting weld residual stresses. The present work seeks to extend this level of understanding to include the effects of the assumed material annealing behaviour, particularly when modelling multi-pass welds that comprise several thermo-mechanical loading cycles. A series of numerical analyses are performed to examine the variability in predicted residual stress profiles for different material models, using a validated finite element model for a three-pass slot weld in AISI 316LN austenitic steel. The material models consider both the work hardening and annealing assumptions for the chosen material. Model sensitivity is established not only from a weld residual stress perspective, but also from an assessment of the post-weld plastic strain accumulated in the weldment. Predictions are compared with indirect measurements acquired using cross-weld micro-hardness maps taken from benchmark specimens. Sensitivity studies reveal that the choice of annealing behaviour will have a significant impact on plastic flow predictions, which is dependent on the annealing temperature specified. Annealing assumptions will have a varying impact on the weld residual stress predictions, such that the extent of sensitivity is dependent on the plasticity model chosen. In contrast, the choice of plasticity model will have a significant effect on the predicted weld residual stresses, but relatively little effect on predictions of equivalent plastic strain.

1. Introduction

Weld residual stresses (WRS) arise as a result of a permanent shape misfit between plastically deformed material near the weld region and the rest of the parent structure. In welding, this misfit is caused by a severe thermal gradient that, due to localised thermal expansion of the heat-affected material, generates plastic deformation in the vicinity of the weld pool (Withers, 2001a). It is of technological importance to know the magnitude and direction of these WRS, as they can superimpose on operational stresses and thus contribute to premature failure of the welded component or structure (Withers, 2001a, 2007). It has also been shown that WRS can provide the driving force for crack initiation and growth (Muránsky et al., 2014), thereby affecting the service lifetime of a welded structure.

In recent years, considerable effort has been dedicated to the standardisation of WRS measurement (Withers, 2001a,b; Hutchings et al., 2005) and prediction in austenitic steel welds (Muránsky et al., 2012a,b; Smith et al., 2012a). Residual stresses in representative benchmark weld specimens have been measured and predicted using a variety of techniques. A round-robin investigation is often used to ensure the highest confidence in the accuracy of each technique; one example of such collaborative effort is the research presented through Task Group 4 (TG4) of the European Network on Neutron Techniques Standardisation for Structural Integrity (NeT) (Muránsky et al., 2012a). Through NeT TG4, a set of AISI 316LN three-pass slot weld benchmark specimens have been produced for WRS measurement and finite element (FE) analysis. The TG4 weld specimens are of particular interest to the nuclear industry, where multi-pass welding processes are often used for austenitic steel weldments and WRS may adversely affect the structural integrity of these welded components.

Both diffraction (neutron and synchrotron X-ray) (Muránsky et al., 2012a; Martins et al., 2010) and stress relaxation

* Corresponding author. Tel.: +61 2 9717 3488; fax: +61 2 9543 7179.
E-mail address: ondrej.muransky@ansto.gov.au (O. Muránsky).

(deep-hole drilling and contour cutting) techniques have been employed for WRS measurement under the NeT TG4 program. These independent WRS measurements were then used in the validation of FE analyses (Muránsky et al., 2012a,b; Dewees et al., 2014). It has been shown that welding simulations developed by ANSTO and EDF Energy in Muránsky et al. (2012a,b) accurately predict WRS in multi-pass 316LN welds, provided the key simulation variables (i.e. material properties and welding parameters) are known. Sensitivity analyses have revealed that the choice of constitutive material response can significantly influence the predicted WRS distribution (Muránsky et al., 2012b). Specifically, it was determined that adopting a mixed (isotropic-kinematic) cyclic plasticity model provides the most accurate prediction of WRS, while using a more conventional (and relatively easy-to-calibrate) isotropic plasticity model provides conservative[1] WRS estimates. Importantly, it was noted in Muránsky et al. (2012b) that different constitutive plasticity theories intrinsically predict different levels of accumulated post-weld plastic strain. Improper characterisation of post-weld plastic strain might have serious consequences if not taken into account because this strain may adversely affect the failure characteristics of welded structures. This level of model accuracy is often overlooked since the validation of numerical weld analyses is traditionally performed via comparison of predicted and measured WRS, with no consideration of accumulated plasticity.

In addition, recent advances in the measurement of accumulated plastic strain present an opportunity to re-examine the accuracy of welding simulations based on this characteristic. Model validation based on an alternate weld feature allows the analyst a more comprehensive assessment of the key simulation variables used in computational weld mechanics. In the present work, post-weld plastic strain in the NeT TG4 benchmark weld specimens is measured using a novel technique, whereby equivalent plastic strain is indirectly characterised using micro-hardness maps. Hence, both post-weld plastic strain and associated post-weld residual stresses are compared with experimental results to establish the accuracy of current weld modelling procedures, providing best-practise recommendations to FE analysts.

In the present work, the sensitivity of plastic strain and WRS predictions is examined when key parameters in the constitutive material model are varied. First, the sensitivity of the numerical solution is examined when isotropic, kinematic and isotropic-kinematic (mixed) plasticity theories are adopted under identical high-temperature annealing conditions. Then, model sensitivity to the assumed high-temperature material annealing behaviour is examined. Model predictions are compared to measurements of both WRS (previously documented in Muránsky et al. (2012a,b)) and accumulated plastic strain in the NeT TG4 benchmark specimens. Since post-weld plastic strain measurements are inferred from calibrated micro-hardness tests, the accuracy of using this novel hardness-based approach for quantifying plastic strain is also assessed in the present study. If successful, such an approach would provide complementary model validation alongside the more traditional WRS assessments.

2. Weld specimen

A series of benchmark weld specimens were manufactured under the auspices of NeT TG4 (Muránsky et al., 2012a; Martins, 2009). Multiple specimens were produced using an identical weld procedure to allow simultaneous WRS measurement as part of an international round-robin examination. Weld design comprises a three-pass ER316L austenitic steel slot weld in solution heat-treated (45 min @ 1050 °C) AISI 316LN austenitic steel plate. The nominal dimensions of the plate, shown in Fig. 1, are 194(l) × 150(w) × 18(h) mm with an 80-mm long and 6-mm deep centreline slot. The slot was filled with three superimposed weld passes via a mechanised Tungsten Inert Gas (TIG) welding process. The specimens were welded free of constraint, allowing the plates to distort without inhibition. Three of the benchmark specimens were instrumented with an array of thermocouples (Muránsky et al., 2012a) to assure welding repeatability and provide transient thermal data for the heat source calibration in numerical analyses. Full details of the welding procedure can be found in Muránsky et al. (2012a).

3. Numerical weld analysis

A sequentially coupled thermo-mechanical FE analysis was performed, whereby the numerical solution from a thermal FE analysis is used as input for a mechanical FE analysis. The thermal model used a representative heat source calibrated using the FEAT-WMT modelling package (Smith, 2010), which was supplied to the ABAQUS 6.13 (SIMULIA, 2014) commercial FE package as a series of time- and spatially-resolved volumetric power densities. Taking advantage of specimen symmetry (see Fig. 1), a 3D half-model comprising 38,220 hexahedral quadratic elements was constructed. Although the parent (AISI 316LN) and filler (ER316L) materials have a slightly different chemical composition (Muránsky et al., 2012a), the same physical[2] and elasto-plastic[3] mechanical properties were used for both materials over the temperature range of interest (25–1500 °C). While a significant volume fraction of metastable δ-ferrite is likely to form at high temperatures upon welding, most of this material transforms back to austenite at a temperature close to the steel melting point. Since the temperatures over which these solid-state phase transformations occur are well above the annealing temperature of the material, they will have a negligible effect on accumulated WRS (Muránsky et al., 2012a; Martins et al., 2010) and plastic strain, and are thus not considered in the present numerical analyses.

Within the constitutive material model used, two key simulation variables have been identified that will significantly affect numerical predictions: (i) *material plasticity theory* (Muránsky et al., 2012b), which describes temperature-dependent material yield and hardening behaviour; and (ii) *material annealing behaviour*, which describes the loss of accumulated plastic strain and thus high-temperature metal softening.[4] The following sections discuss each simulation variable in greater detail.

3.1. Material plasticity theories

The most commonly employed constitutive plasticity theories used in computational weld mechanics are isotropic plasticity theory, kinematic plasticity theory and isotropic-kinematic (i.e. mixed) plasticity theory (Muránsky et al., 2012b). These theories differ in the way they capture the response of the material to cyclic loading, in both the material yield and work-hardening behaviour. Variations in how each theory simulates cyclic loading is shown schematically in Fig. 2. The characterisation of material yield and work hardening behaviour under reverse loading has a profound effect on the prediction of WRS and plastic strain. This effect is particularly true for multi-pass welds, since the material in the

[1] When peak tensile WRS are over-predicted using an isotropic hardening model, these stresses may subsequently create large compressive equilibrating stresses, which are typically non-conservative from a structural integrity standpoint.

[2] Density (ρ), thermal conductivity (λ), and specific heat (c_p).

[3] Young's modulus (E), Poisson's ratio (ν), and work-hardening behaviour.

[4] Softening refers to a reduction of the work hardening rate and/or the yield strength of the material.

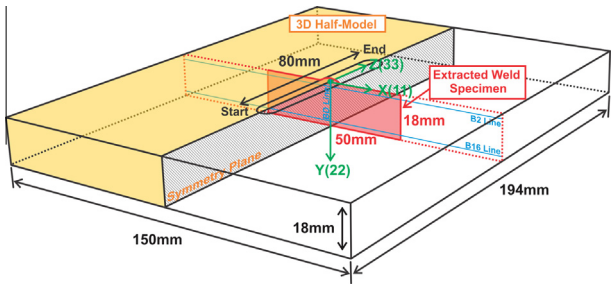

Fig. 1. NeT TG4 weld geometry, showing the symmetry plane for the finite element simulations, the location of the extracted cross-weld specimen for hardness measurements, and the line profiles (BD, B2, B16) along which the post-weld residual stresses and post-weld plastic strain were measured.

vicinity of weld undergoes multiple thermo-mechanical loading cycles during the welding process.

Isotropic plasticity theory allows the uniform dilation of the yield surface about its centre while maintaining its shape, orientation and centroid position in stress space. The equivalent stress defining the size of the yield surface (σ^0) can be defined as follows:

$$\sigma^0 = \sigma|_0 + Q_{inf}\left(1 - e^{-b\bar{\varepsilon}^{pl}}\right), \tag{1}$$

where $\sigma|_0$ is the equivalent yield stress when the equivalent plastic strain ($\bar{\varepsilon}^{pl}$) is 0; and Q_{inf} and b are temperature-dependent material parameters. Kinematic hardening allows the yield surface to translate in stress space while maintaining its shape, size and orientation. It is defined by an additive combination of a linear hardening term and a nonlinear relaxation term, such that

$$\dot{\boldsymbol{\alpha}} = \sum_i \left[C_i \frac{1}{\sigma^0}(\boldsymbol{\sigma} - \boldsymbol{\alpha})\dot{\bar{\varepsilon}}^{pl} - \gamma_i \boldsymbol{\alpha}\dot{\bar{\varepsilon}}^{pl}\right], \tag{2}$$

where $\dot{\boldsymbol{\alpha}}$ represents the hardening rate of the backstress tensor $\boldsymbol{\alpha}$; $\boldsymbol{\sigma}$ is the applied stress tensor; and C_i and γ_i are material constants. When mixed hardening is considered, the size of the yield surface due to isotropic hardening (σ^0, Eq. (1)) is used instead of $\sigma|_0$ when defining the kinematic hardening rate in Eq. (2).

It is important to highlight the functionality of Eqs. (1) and (2) in this work, since the distinction must be made between (i) material annealing behaviour controlled by ABAQUS using $\bar{\varepsilon}^{pl}$ (i.e. ABAQUS variable PEEQ), and (ii) softening behaviour dictated by material constants (Q_{inf} and C_i). For example, isotropic softening is enforced by setting Q_{inf} to 0 at temperatures above 900 °C based on experimental tests (Smith et al., 2009; Smith, 2006). While this setting forces the yield surface back to its original size $\sigma|_0$, the accumulated plastic flow in the material is maintained; hence, prior work hardening is kept and the material has not annealed. A similar effect can be observed for kinematic hardening; C_i has been set to 0 at temperatures above 1000 °C (Smith et al., 2009; Smith, 2006), such that only the nonlinear relaxation term in Eq. (2) is active as plastic strain continues to accumulate. As discussed below, specification of an annealing temperature in ABAQUS will set $\bar{\varepsilon}^{pl}$ (and consequently, $\dot{\bar{\varepsilon}}^{pl}$) to 0 such that all accumulated plastic strain is lost once this temperature is exceeded. This annealing will cause a similar isotropic softening via Eq. (1), while no kinematic relaxation will occur due to Eq. (2). This distinction is important since we are concerned in this work with annealing phenomena, and not material softening due to the lower activation energy required for plastic flow at elevated temperatures (governed by Q_{inf} and C_i).

3.2. Material annealing behaviour

High-temperature annealing is an important phenomenon that needs to be accounted for in any welding simulation. The annealing behaviour of a material is typically defined by setting a temperature above which the material loses all accumulated plastic strain. This loss of plasticity naturally leads to the relaxation of the associated stresses in the annealed region when isotropic hardening is considered (Eq. (1)), as the material is no longer in a work-hardened state. For kinematic models (Eq. (2)), stresses will remain constant since no additional plastic strain is accumulated during annealing ($\dot{\bar{\varepsilon}}^{pl} = 0$). In the present study, two different assumptions on how to capture annealing behaviour during welding are examined:

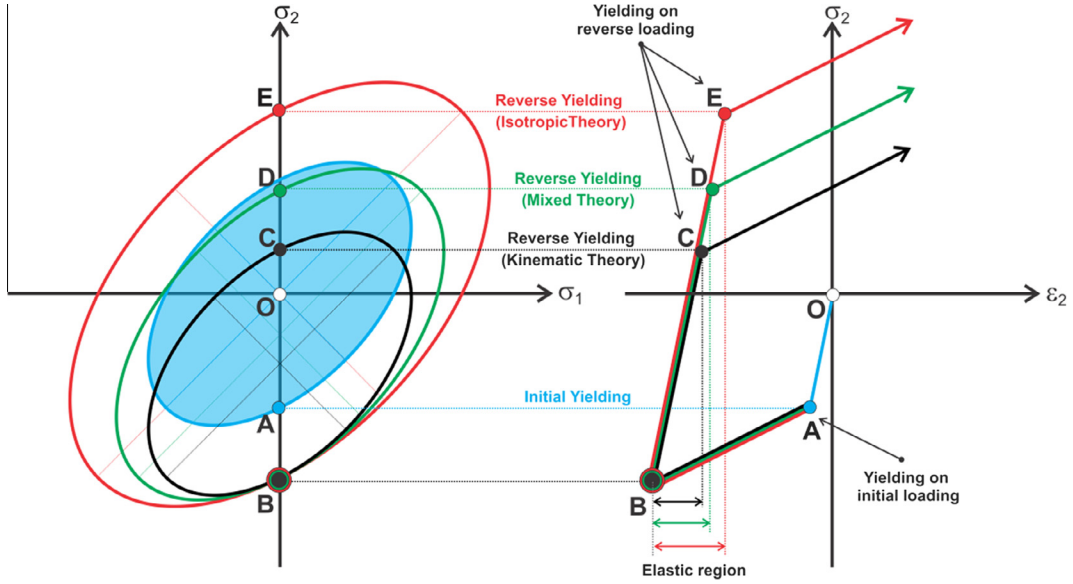

Fig. 2. The effect of isotropic, kinematic and isotropic-kinematic (mixed) plasticity theory on predicting initial yield and cyclic yield. (i) Isotropic theory allows the expansion of the initial yield surface, (ii) kinematic theory allows translation of the initial yield surface, and (iii) mixed theory allows both expansion and translation of the initial yield surface. *A* = initial yield; *B* = post-yield work hardening; *C*, *D*, *E* = yield on reverse loading, as predicted by kinematic, mixed and isotropic plasticity theory respectively.

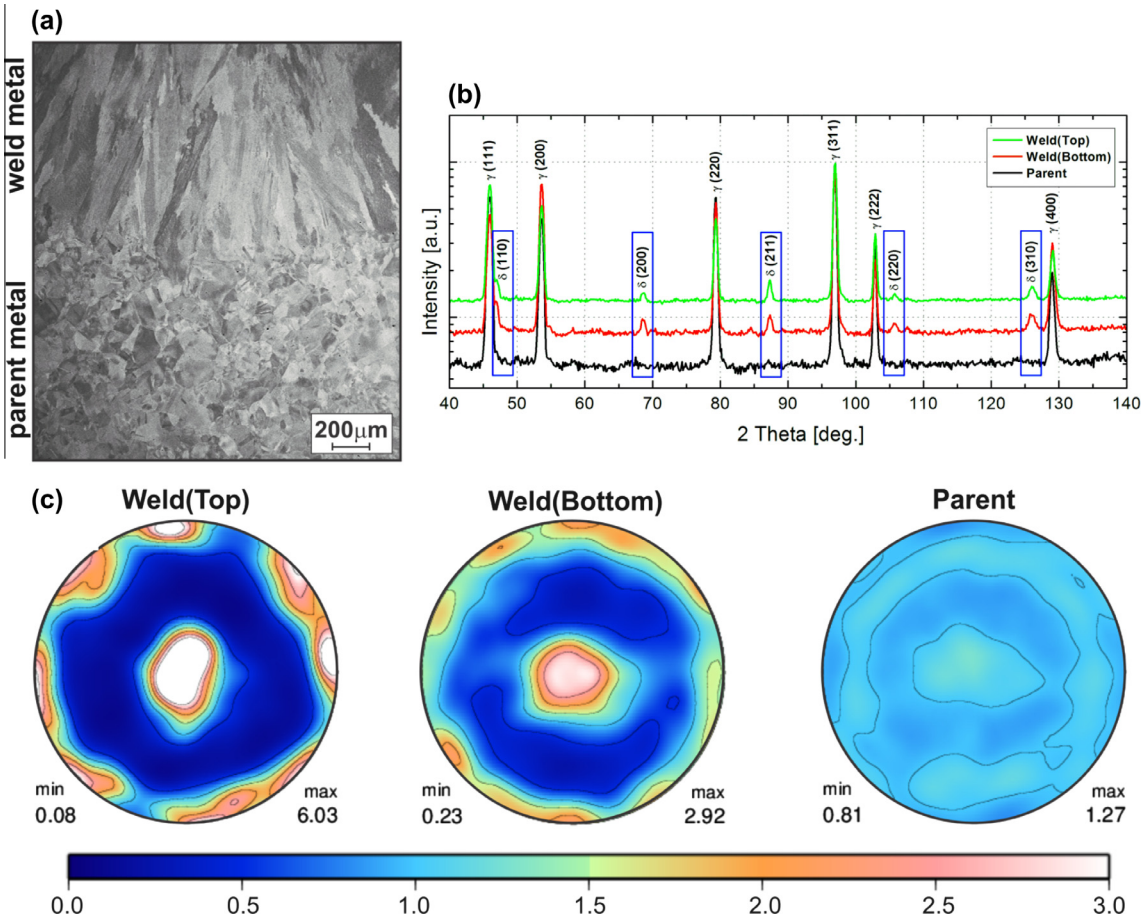

Fig. 3. The microstructural differences between weld and parent metal, identified using several techniques on a NeT TG4 specimen. (a) Optical macrograph highlighting the variation in grain dimensions between the weld and parent metal. (b) Neutron diffraction patterns obtained using the ECHIDNA high-resolution powder diffractometer at ANSTO, showing diffraction peaks corresponding to fcc γ-phase (austenite) and bcc δ-phase (ferrite) in the weld region. This diffraction data reveals the existence of δ-ferrite in the weld region, while no δ-ferrite is present in the parent metal. (c) Bulk texture measurement, comprising {200} pole figures of weld and parent metal, obtained using the KOWARI strain diffractometer at ANSTO. The texture shows preferential solidification texture formed in the weld metal, while parent metal texture is fairly random.

1. *A single-stage annealing assumption*, with a single annealing temperature (T_0). In this case, any temperature rise above T_0 causes the accumulated plastic strain (represented in ABAQUS using the equivalent plastic strain, PEEQ[5]) at a material integration point to be set to zero, thus eliminating all plastic history.
2. *A two-stage isotropic annealing approach*, whereby two annealing temperatures (T_1, T_2) capture the progressive nature of annealing processes more accurately. At temperatures between the lower annealing temperature (T_1) and the upper annealing temperature (T_2), the material is prevented from any further hardening by holding the accumulated plastic strain constant. At temperatures above T_2, the material loses all accumulated plastic strain (i.e. PEEQ = 0) in a similar manner to single-stage annealing. Full details of two-stage annealing functionality within ABAQUS/Standard are given in ABAQUS (2007).

4. Experimental characterisation

The cross-weld macrograph in Fig. 3(a) shows that the weld metal is comprised of relatively large dendritic grains, which is very different from the smaller equiaxed grains present in the parent metal. Additional phase analysis, shown in Fig. 3(b) using the ECHIDNA high-resolution diffractometer at ANSTO (Liss et al., 1010), revealed approximately 5% (by volume) δ-ferrite exists in the weld metal that is not present in the parent metal. This measurement agrees with phase predictions via the Schaeffler diagram (Shchaeffler, 1949), which take into consideration the higher Cr content in the weld filler metal. The higher Cr content in the weld metal (19 wt%) over the parent metal (17.5 wt%) also suggests an increased hardenability of the weld (Muránsky et al., 2012a). Finally, bulk texture measurements presented in Fig. 3(c) show that the textures measured for weld and parent metals are markedly different. Weld metal texture is considerably stronger, with the {100} plane-normals oriented towards the sample normal direction (Y(22), Fig. 1) (i.e. the direction of the heat flow). In contrast, the parent metal texture is fairly random. These microstructural variations are expected to affect the mechanical properties of each material, thus influencing experimental measurements of both post-weld plastic strain and WRS. Significant work has been performed in an attempt to properly capture the constitutive weld metal behaviour; the best results to date have been achieved using solution-annealed weld metal tensile specimens (Smith et al., 2012b). In the present work, cross-weld microstructural variations have not been explicitly considered in experimental measurements, which may lead to some deviation in measured data that has yet to be quantified. [6]

[5] PEEQ = $\bar{\varepsilon}^{pl}|_0 [(\sqrt{2/3}\dot{\boldsymbol{\varepsilon}}^{\boldsymbol{pl}} : \dot{\boldsymbol{\varepsilon}}^{\boldsymbol{pl}})\mathrm{d}t]^t$, where $\bar{\boldsymbol{\varepsilon}}^{\boldsymbol{pl}}|_0$ is initial equivalent plastic strain and $\dot{\boldsymbol{\varepsilon}}^{\boldsymbol{pl}}$ is the plastic strain tensor at time t. In the present work, the initial equivalent plastic strain is set to zero because the plate was solution heat-treated prior to welding.

[6] Sensitivity analyses would also need to consider the accuracy of the fitting technique used on cyclic loading test data, which may considerably influence weld model accuracy. Such work is outside the scope of this study.

4.1. Characterisation of plastic strain via micro-hardness measurement

Plastic deformation in the vicinity of the weld was characterised using cross-weld micro-hardness measurements. A Nano Indenter G300 (Keysight) with a Berkovich tip was used, and measurements were taken under Continuous Stiffness Mode (CSM). The hardness measurements in Fig. 4(a) converge asymptotically to a true hardness value of ~200 Hv at imprint depths greater than 2.0 μm; these indent depths are proportional to the applied indent load for measurement. Fig. 4(b) shows typical load–displacement curves for the 316LN parent metal using the 30-gf indent load specified; the indent depth (2.35 μm) is sufficient to overcome the size effects illustrated in Fig. 4(a), thus this load is used for generation of micro-hardness map data.

The 2(L) × 50(T) × 18(N)-mm sample used for micro-hardness measurements was extracted via electro-discharge machining (EDM) from the weld mid-length, as shown schematically in Fig. 1. The measured hardness map of this sample is presented in Fig. 5(a). A motorised *X*–*Y* stage mounted on the indenter gave a precise spatial resolution of 0.5 mm (i.e. ΔX, ΔY = 0.5 mm). To convert the measured micro-hardness to calculated plastic strain (PEEQ), a relationship between micro-hardness and plasticity in AISI 316L austenitic steel has been established using a novel tensile specimen (shown in Fig. 6) and the method outlined in Ben Moussa (2013). The amount of plastic deformation along the sample tensile axis was measured using Digital Image Correlation (DIC). A plot of the variation in plastic strain along the sample tensile axis is presented in Fig. 6(a). The corresponding micro-hardness was characterised using the same hardness machine, indenter and load as was used for weld characterisation in the present work; this profile is shown in Fig. 6(b). The consequent relationship between the hardness and plastic deformation along the tensile axis of the specimen is presented in Fig. 6(c). Assuming hardness is directly proportional to yield strength under monotonic tensile loading, the relationship shown in Fig. 6(c) has been fit assuming the formulation of Eq. (1) holds. A good fit can be observed in Fig. 6(c). The relationship was then used to convert the measured post-weld micro-hardness into post-weld plastic strain as presented in Fig. 5(b). This indirect measurement of plastic strain was then used to validate FE predictions.

4.2. Measurement of post-weld residual stresses

A number of residual stress measurement techniques were employed in the NeT TG4 round-robin project; neutron diffraction and spiral-slit synchrotron diffraction measurements are presented here. Neutron diffraction residual stress measurements were carried out using the KOWARI diffractometer at ANSTO (Muránsky et al., 2012a; Brule et al., 1040), while synchrotron diffraction residual stress measurements were carried out using ID-15 at ESRF (Martins et al., 2010). It is important to note that while the neutron diffraction technique can access strain components in all three principal strain directions, the synchrotron diffraction technique can access only two principal strain components; the calculation of principal stresses from strain data must be done assuming plane stress conditions exist through the sample thickness. The validity of such an assumption for the current sample geometry has been previously confirmed in Muránsky et al. (2012a) and Martins et al. (2010).

5. Results and discussion

Figs. 7 and 8 present contour plots of the predicted longitudinal (σ_{33}) post-weld residual stresses (WRS) and post-weld plastic strain (via PEEQ) respectively, in the vicinity of the weld at the weldment mid-length (see Fig. 1) for the following model assumptions:

(1) Isotropic plasticity theory, single-stage annealing, T_0 = 1050 °C,
(2) Isotropic plasticity theory, single-stage annealing, T_0 = 1300 °C,
(3) Kinematic plasticity theory, single-stage annealing, T_0 = 1050 °C,
(4) Isotropic-kinematic (mixed) plasticity theory, single-stage annealing, T^0 = 1050 °C,

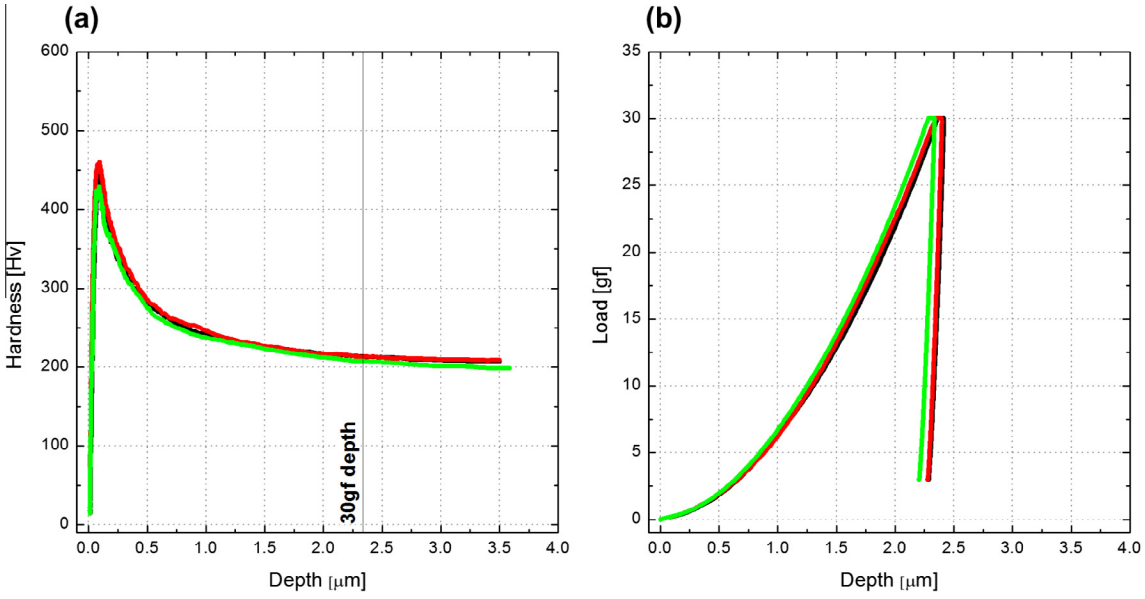

Fig. 4. (a) Continuous Stiffness Mode (CSM) hardness measurements showing the effect of depth of indent, which is proportional to the applied load, on the measured micro-hardness. Size effects are overcome at indent depths greater than 2.0 μm. (b) CSM load–displacement data for a 30-gf indent load, revealing the indent depth (2.35 μm) is sufficient for accurate hardness measurements.

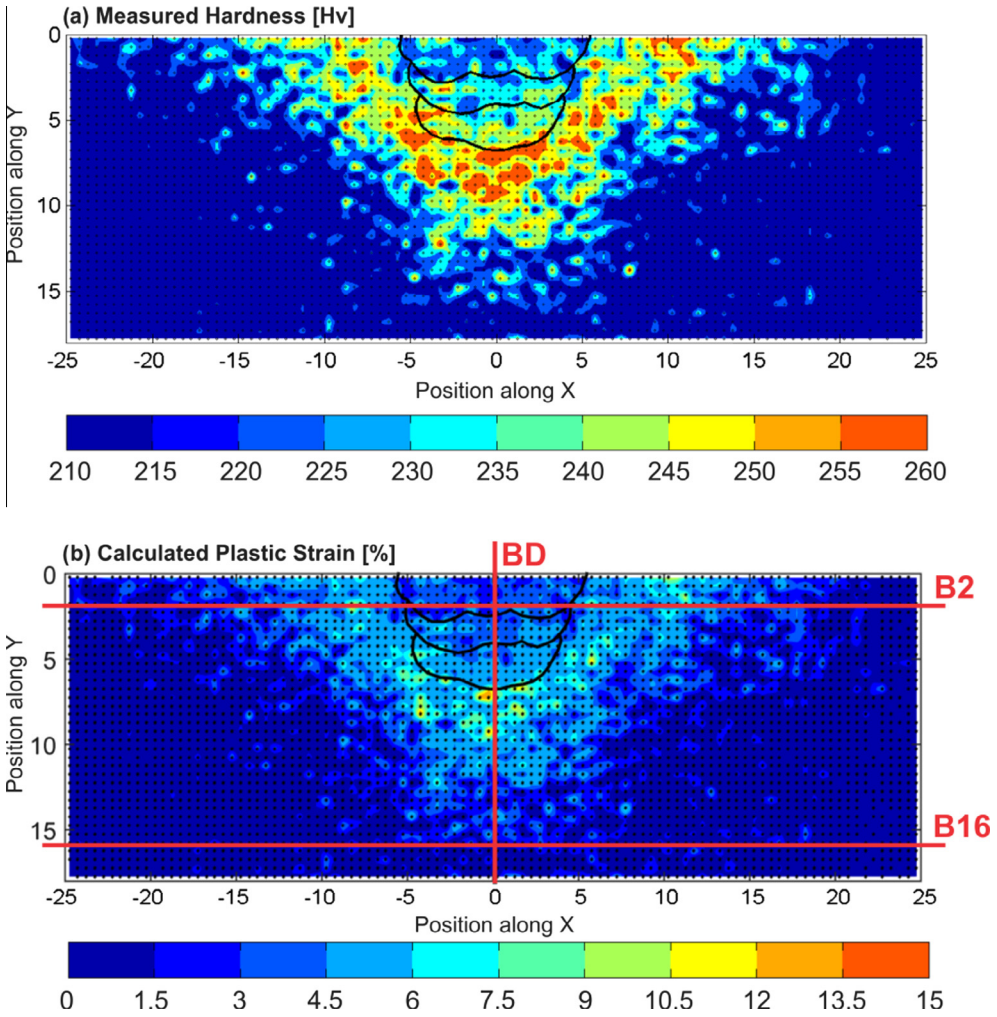

Fig. 5. (a) Map of measured Vickers hardness obtained using micro-indentation, with a Berkovich tip and an indent load of 30 gf. The spatial resolution of is map is 0.5 mm. (b) Post-weld plastic strain calculated using the established hardness-plasticity relationship shown in Fig. 6(c).

(5) Isotropic-kinematic (mixed) plasticity theory, single-stage annealing, T_0 = 1300 °C,
(6) Isotropic-kinematic (mixed) plasticity theory, two-stage annealing, T_1 = 800 °C, T_2 = 1300 °C.

Only the longitudinal stresses are present here as they are of the highest magnitude (Muránsky et al., 2012a,b; Martins et al., 2010) and are consequently the most sensitive to any model assumption. Because the model is symmetric along the weld centreline (Fig. 1), half-model results are present in Figs. 7 and 8 under the assumption that these results are reflected on the opposite side of the specimen. To validate this assumption, all measurements were taken on either side of the weld centreline, along a series of lines as presented in Figs. 9 and 10. Data from three line profiles are presented in this work (with locations shown in Figs. 1, 7 and 8):

Line BD: Line BD runs through the plate-thickness at the centre of the TG4 benchmark specimen. This line crosses a number of important isotherms: (i) the 1400 °C isotherm, defining the fusion boundary; (ii) the 1050°C and 1300 °C isotherms that define the single-stage annealing temperatures assumed in this study; and (iii) the 800 °C and 1300 °C isotherms that define the lower and upper annealing temperatures used under a two-stage annealing assumption. While symmetry assumptions cannot be seen using this profile (since it runs along the symmetry plane), it illustrates the effect of thermo-mechanical cyclic loading on the constitutive material response.

Line B2: Line B2 runs perpendicular to the weld at the mid-length of the plate, 2 mm below the top plate surface. All of the isotherms represented along line BD are represented here; however, line B2 will only traverse the weld metal deposited during the last weld pass (PASS.3 in Figs. 9 and 10). As such, data collected within the weld bead along this line reflects the material response to monotonic loading on cooling (Muránsky et al., 2012b). The cross-weld measurements along this profile will be able to confirm symmetry assumptions.

Line B16: As with line B2, line B16 runs perpendicular to the weld at the mid-length of the plate. This line runs 16 mm below the top plate surface; as such, it passes solely through the parent metal. From this position, it is possible to examine the cross-weld material response when subjected to all three thermo-mechanical loading cycles, allowing ready comparison to the monotonic loading behaviour of the weld metal observed along line B2. Symmetry assumptions within the parent metal may also be validated along this line.

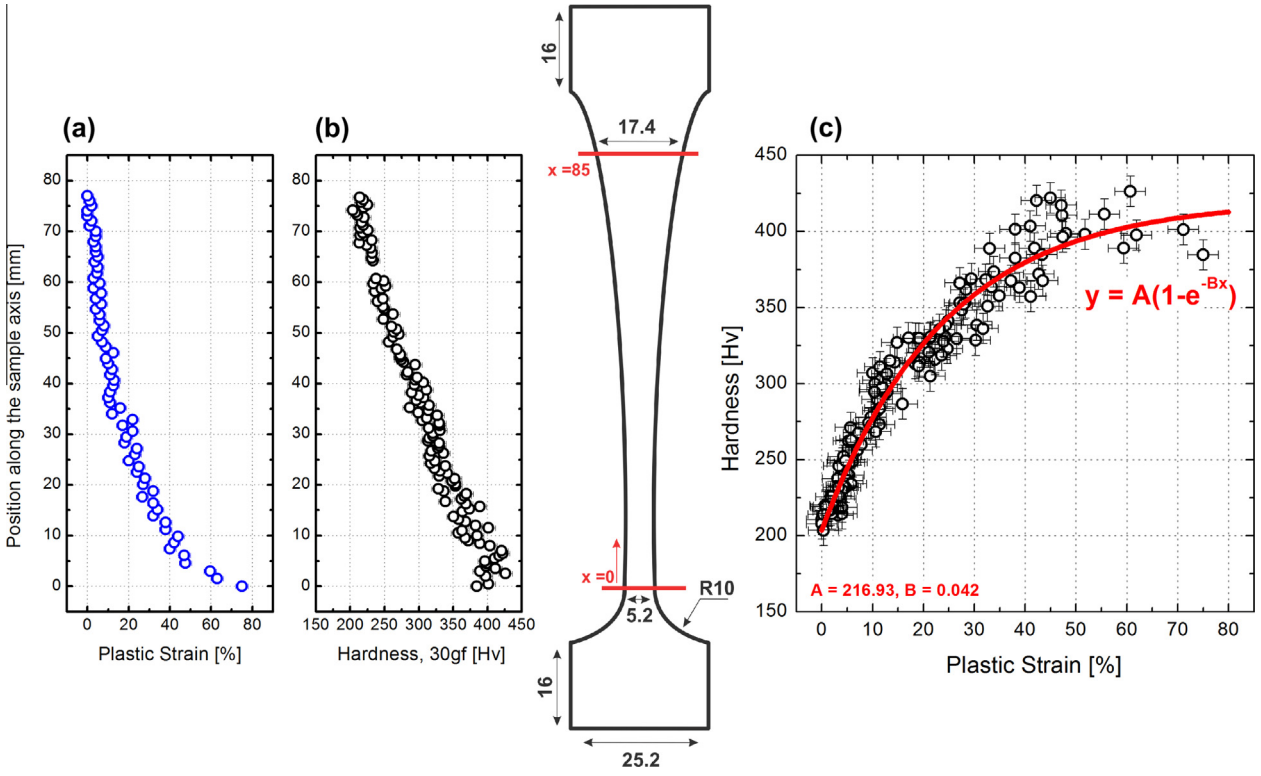

Fig. 6. Method of defining a relationship between plastic strain and micro-hardness in AISI 316L material, using a novel tensile specimen (shown centre of figure). (a) Plastic strain measurements along the sample loading axis, obtained via Digital Image Correlation (see Ben Moussa, 2013 for details). (b) Hardness measurements along the sample loading axis obtained using micro-indentation, with a Berkovich tip and an indent load of 30 gf. (c) Relationship between the plastic strain and hardness for AISI 316L.

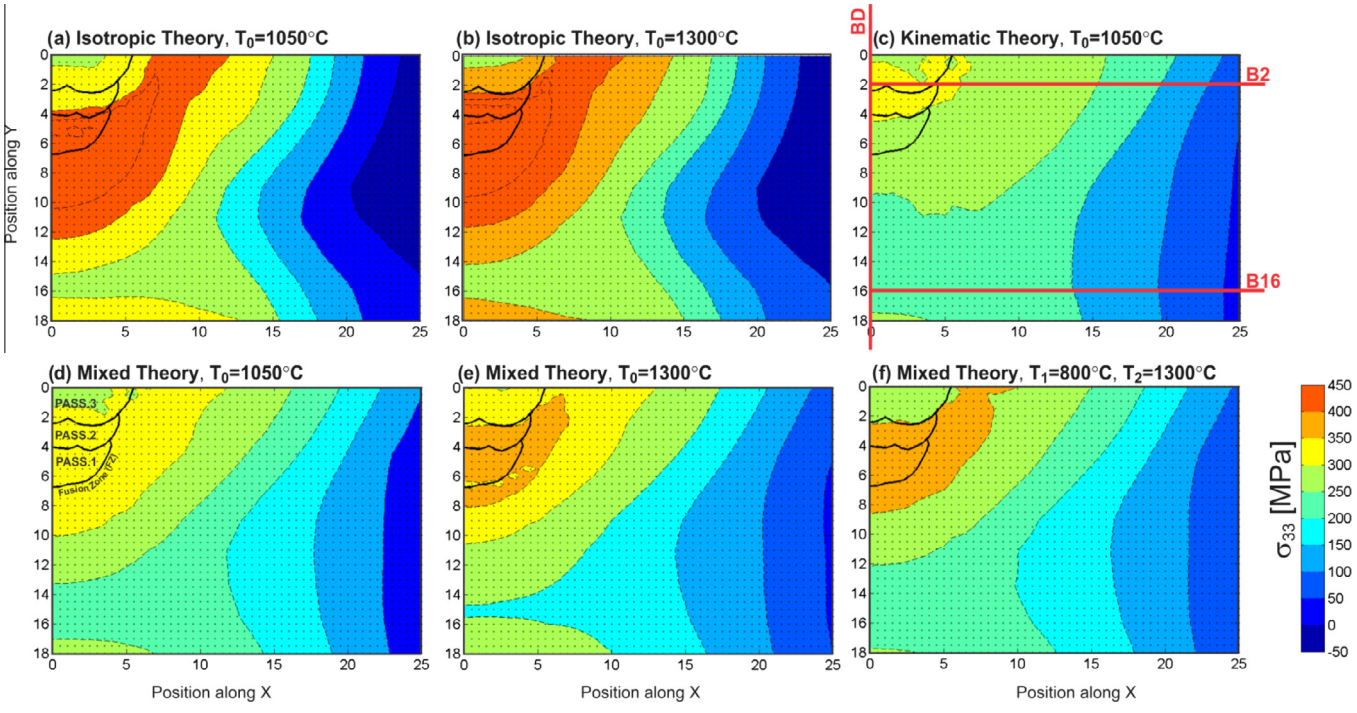

Fig. 7. 2D maps of predicted longitudinal WRS in the steady-state region in the mid-length of the TG4 specimen. (a) Isotropic plasticity model with a single-stage annealing assumption: T_0 = 1050 °C. (b) Isotropic plasticity model with a single-stage annealing assumption: T_0 = 1300 °C. (c) Kinematic plasticity model with a single-stage annealing assumption: T_0 = 1050 °C. (d) Mixed plasticity model with a single-stage annealing assumption: T_0 = 1050 °C. (e) Mixed plasticity model with a single-stage annealing assumption: T_0 = 1300 °C. (f) Mixed plasticity model with a two-stage annealing assumption: T_1 = 800 °C; T_2 = 1300 °C.

Before assessing model sensitivity to key simulation variables, several features of both the measurements and the predictions present in Figs. 9 and 10 must be discussed:

1. Both the WRS and plastic strain measurements along lines B2 and B16 are symmetric along the symmetry plane, which validates the use of an FE half-model (Muránsky et al., 2012a).

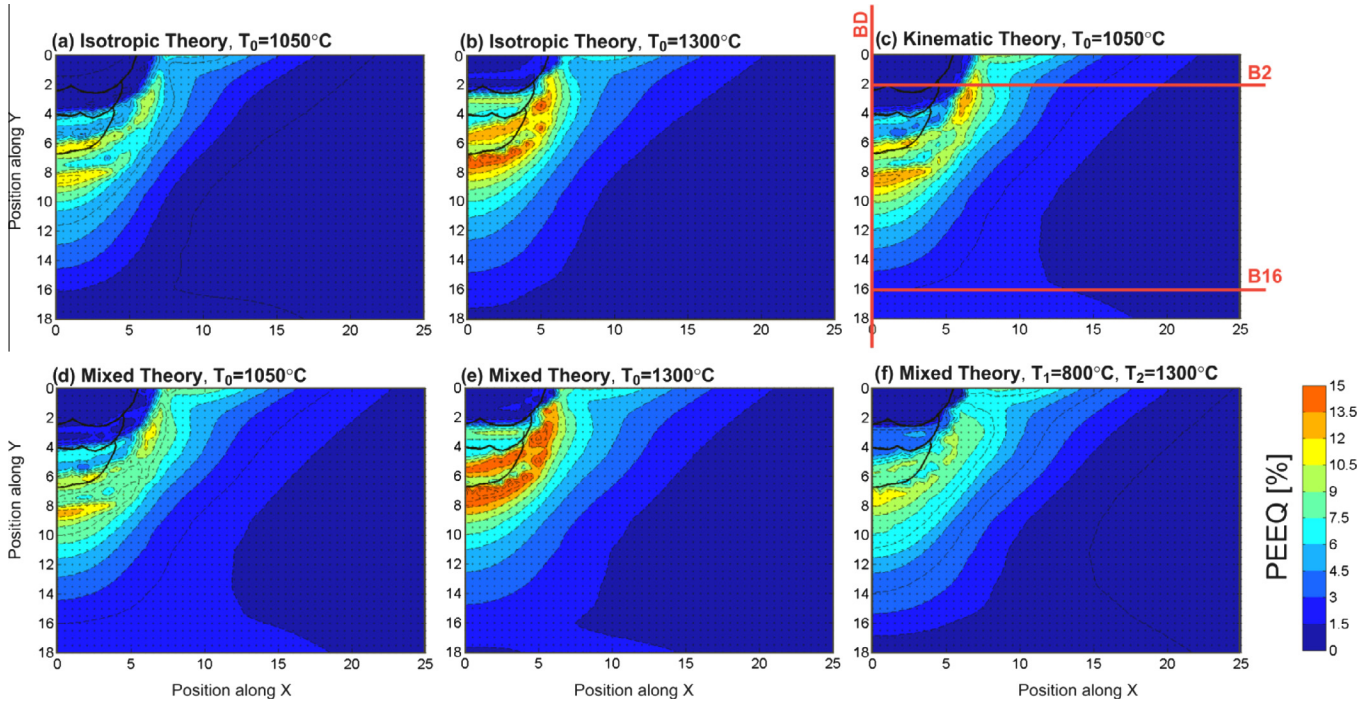

Fig. 8. 2D maps of predicted post-weld strain (PEEQ) in the mid-length steady-state region of the TG4 specimen. (a) Isotropic plasticity model with a single-stage annealing assumption: T_0 = 1050 °C. (b) Isotropic plasticity model with a single-stage annealing assumption: T_0 = 1300 °C. (c) Kinematic plasticity model with a single-stage annealing assumption: T_0 = 1050 °C. (d) Mixed plasticity model with a single-stage annealing assumption: T_0 = 1050 °C. (e) Mixed plasticity model with a single-stage annealing assumption: T_0 = 1300 °C. (f) Mixed plasticity model with a two-stage annealing assumption: T_1 = 800 °C; T_2 = 1300 °C.

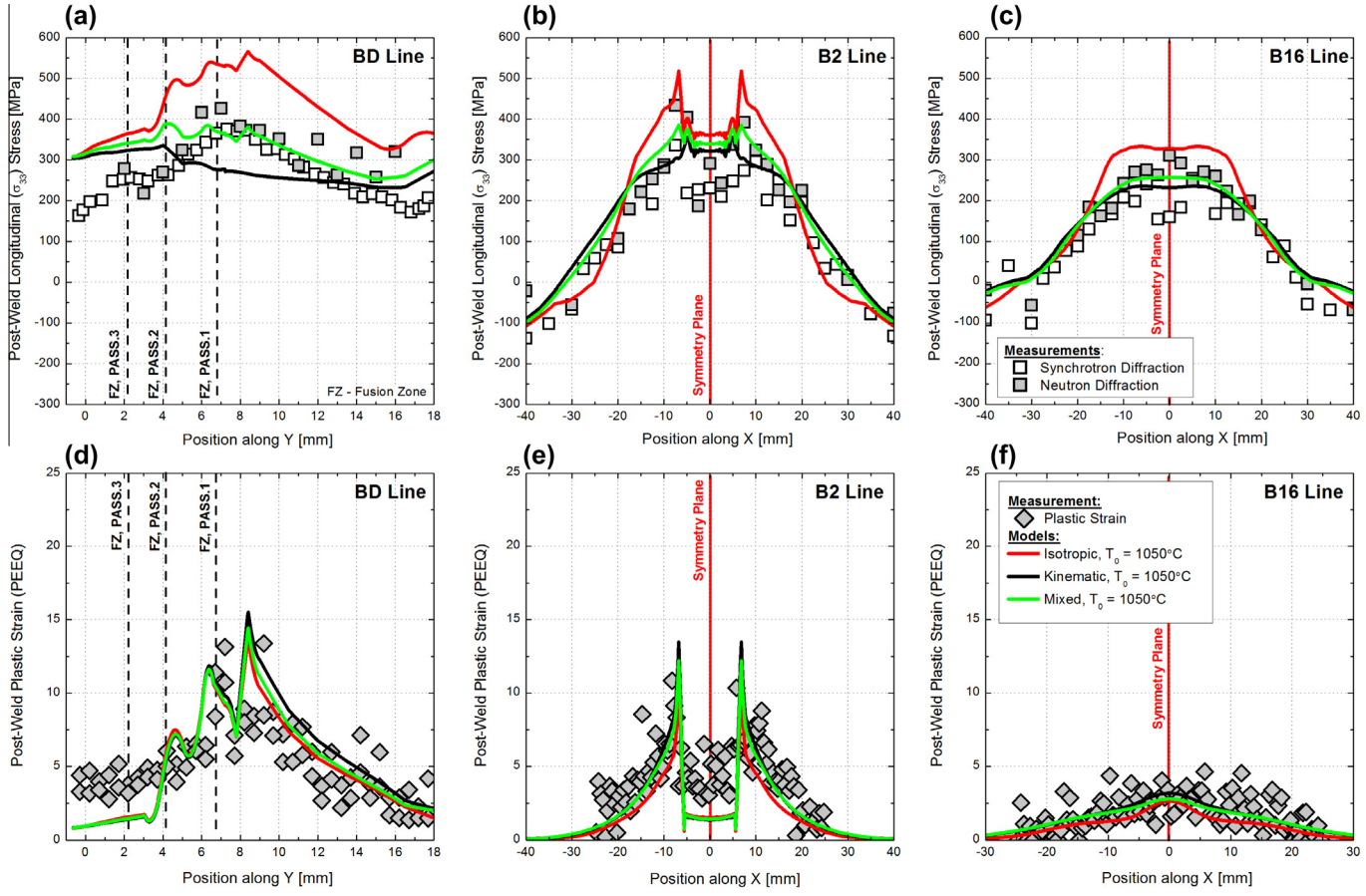

Fig. 9. Comparison of the predicted WRS and post-weld plastic strain along line BD (a,d), line B2 (b,e) and line B16 (c,f) obtained using isotropic, kinematic and mixed plasticity theory with single-stage annealing assumption (T_0 = 1050 °C). WRS predictions are shown alongside synchrotron (open symbol) and neutron (solid symbol) diffraction measurements; the error associated with the experimental data is approximately 40 MPa. Plastic strain predictions are shown alongside indirect plasticity calculations using micro-hardness measurements; the error associated with this data has not been confirmed.

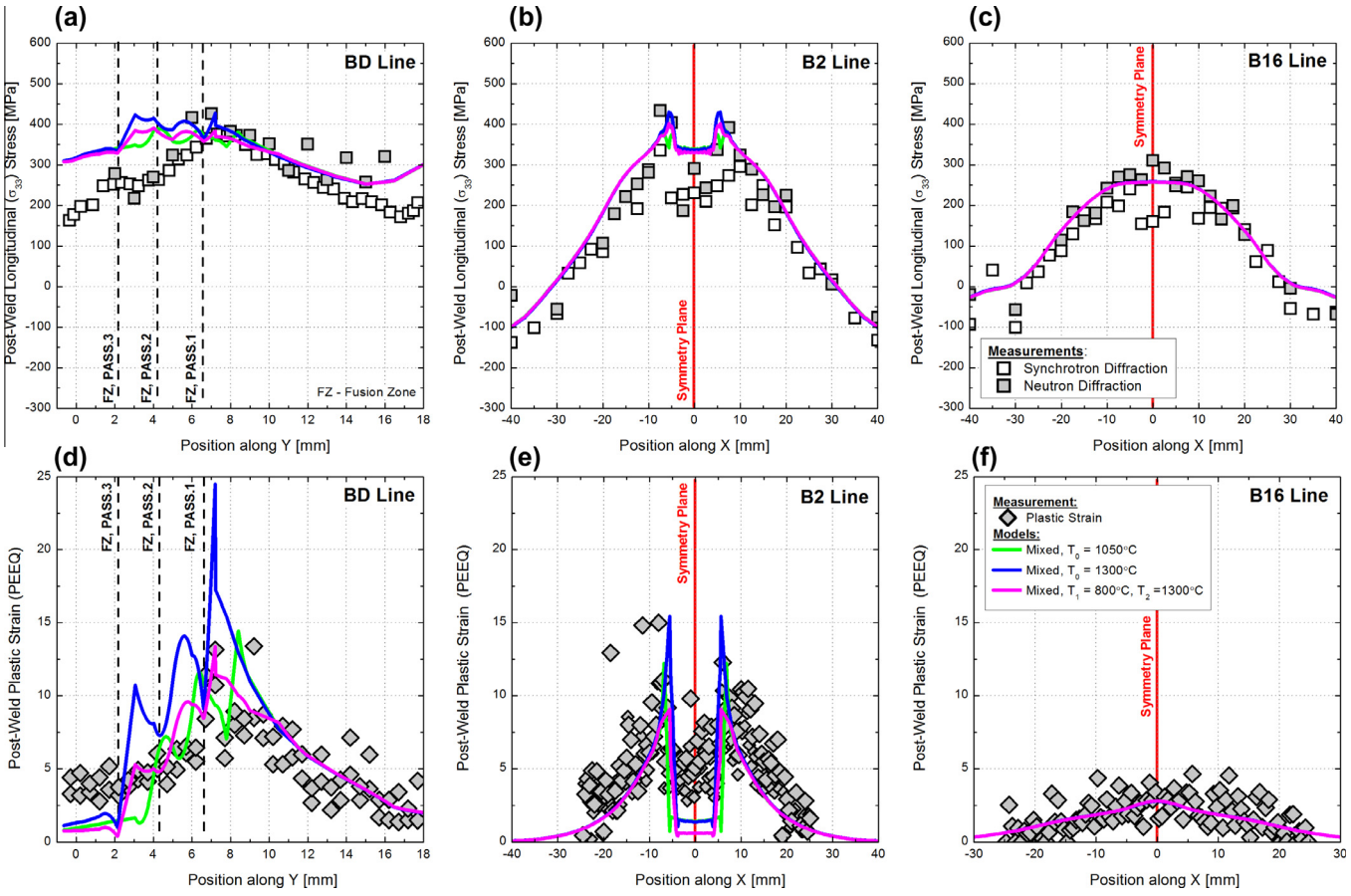

Fig. 10. Comparison of the predicted WRS and post-weld plastic strain along line BD (a,d), line B2 (b,e) and line B16 (c,f). Predictions are obtained using mixed plasticity theory with single-stage annealing assumptions (T_0 = 1050 °C, T_0 = 1300 °C) and a two-stage annealing assumption (T_1 = 800 °C, T_2 = 1300 °C). WRS predictions are presented alongside synchrotron (open symbol) and neutron (solid symbol) diffraction measurements; the error associated with the experimental data is approximately 40 MPa. Plastic strain predictions are shown alongside indirect plasticity calculations using micro-hardness measurements; the error associated with this data has not been confirmed.

2. The WRS profiles measured using both neutron and synchrotron diffraction techniques are in good agreement, providing a high degree of confidence in the measured residual stresses (Muránsky et al., 2012a). This level of confidence cannot be claimed for the plasticity measurements however, since a complementary measurement technique has not yet been used on these samples.
3. WRS predictions are in general agreement with measurements (Figs. 9 and 10). The only notable deviation from measurement lies within the weld metal, where all models tend to over-predict WRS. This deviation increases with each additional weld pass, and is particularly visible in the weld regions of PASS.2 and PASS.3. Since we have a high level of confidence in the measurements (even though only single phase stress analysis was considered in the diffraction measurement techniques (Muránsky et al., 2012a; Martins et al., 2010)), it is most likely that the yield strength of the weld metal has not been accurately represented in the model. Since only the parent material properties are used in the current FE analysis, the over-prediction of WRS in the weld metal suggests that the weld metal has a lower yield strength relative to the parent metal. This would be expected from the considerably coarser microstructure of the weld metal, as shown in Fig. 3(a). An increasing deviation in the predicted WRS exists since deviations in the shape misfit predicted for each weld pass are cumulative. Nevertheless, these inaccuracies do not detract from the present sensitivity study because the model errors they create do not affect model sensitivity results.

Post-weld plastic strain predictions (via PEEQ) are also in general agreement with measured data (Figs. 9 and 10). As with the WRS profiles, there is a discrepancy between measured and predicted data that is most notably visible in the PASS.2 and PASS.3 weld metal. However, unlike the WRS measurements, we cannot be confident that this difference is due to model inaccuracy; in fact, it is likely that the indirect strain measurements are inaccurate in this area. Likely sources of error include the microstructural variations (see Section 4) between weld and parent metals, which may lead to a different hardness-plasticity relationship than that shown in Fig. 6. The aforementioned variations in grain size and shape, in chemical/phase composition, and in bulk texture will influence the hardness-plasticity relationship that was fitted to the parent metal.

An additional source of error in this comparison is that inferring a relationship between hardness and plastic strain from a monotonic test will not provide an exact relationship when a complex (e.g. cyclic) strain path has been applied to the specimen. This relationship is indeed simplified relative to other work (e.g. the cross-weld studies of Smith et al. (2012a)), since the influence of backstress (α) on the yield strength of material subject to cyclic loading is not considered. Here, the accuracy of such a simplification has been assessed. Two important observations from this assessment can be made:

1. PEEQ predictions (under identical annealing behaviour) using isotropic, kinematic, and mixed hardening models are nearly identical in the weld and HAZ material – see Fig. 9(d). This

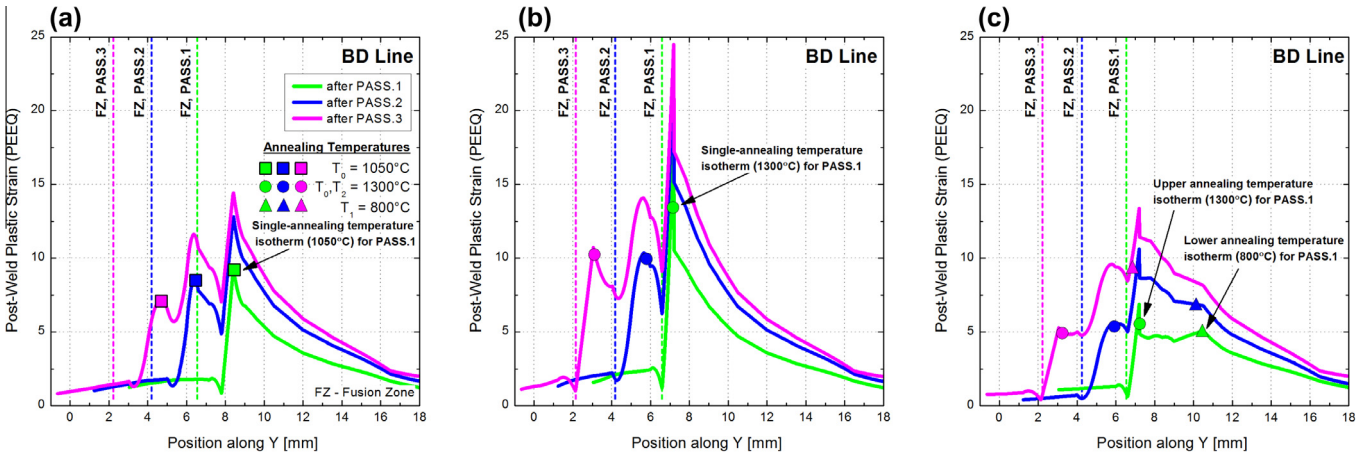

Fig. 11. Comparison of the predicted post-weld plastic strain along line BD, broken into a pass-by-pass analysis. (a) Mixed plasticity theory with a single-stage annealing assumption: $T_0 = 1050$ °C. (b) Mixed plasticity theory with a single-stage annealing assumption: $T_0 = 1300$ °C. (c) Mixed plasticity theory with a two-stage annealing assumption: $T_1 = 800$ °C; $T_2 = 1300$ °C. Locations of the relevant isotherms after each pass are shown to identify the onset of material annealing in the analysis.

similarity implies the inclusion of a backstress tensor in the plasticity model used will not significantly affect the PEEQ predictions of the FE model. The largest variation in PEEQ predictions occurs in the parent metal; however, even in this region the variation is less than the scatter observed in hardness-inferred measurements. This observation tells us that if we can find a way to accurately measure PEEQ, it can be used reliably to assess the validity of an assumed material annealing behaviour for weld simulation.

2. The greatest variation between inferred plasticity measurement and calculated PEEQ profiles occurs (i) in the weld metal deposited on the last pass and (ii) in the adjacent high-temperature HAZ from PASS.2 (Fig. 9(d)). If we focus on the measured data in this region, we see that the inferred plasticity (hence, the hardness) across the weld metal and into the HAZ are relatively constant. This trend implies that the potential for significant backstress in the HAZ to increase the measured hardness (thus the inferred plastic strain) is not observed; otherwise, we would see a significant increase in the measured hardness of the PASS.2 HAZ metal relative to PASS.3 weld metal.

These results indicate it is the microstructural effects and not the monotonic simplification that produce the greatest source of measurement error in the present study. Neglecting the influence of backstress seems to be an acceptable source of error, since the authors have consequently reached a similar conclusion reached by Smith et al. (2012a), who consider backstress in their study of the cross-weld variation in yield strength in a three-pass groove weld specimen (Turski et al., 2009). While these results indicate a source of measurement error exists within the FZ and HAZ regions of the weldment, the numerical sensitivity study with respect to annealing temperature can be assumed valid.

5.1. Model sensitivity to the assumed material plasticity theory

Contour plots in Fig. 7(a–c) and line profiles in Fig. 9(a–c) clearly show that the choice of plasticity theory has a significant effect on the predicted WRS, as previously identified in Muránsky et al. (2012b). This effect is less pronounced for the predictions of post-weld plastic strain shown in Fig. 8(a–c), but it appears that models using isotropic plasticity theory predict a lower-bound plastic strain profile, while models using kinematic plastic theory predict an upper-bound plastic strain profile. This claim is quantitatively supported in the line profiles shown in Fig. 9(d–f), particularly within the parent metal ($Y > 8$ mm on line BD) where the highest amount of plastic strain is expected (Muránsky et al., 2012b). These bounding results arise since isotropic plasticity theory over-predicts the material yield strength under cyclic loading, consequently over-predicting the elastic region (shown schematically in Fig. 2) and under-predicting the amount of plastic strain (PEEQ). In contrast, kinematic plasticity theory under-predicts the material yield strength under cyclic loading, thus under-predicting the elastic region and over-predicting post-weld plastic strain. The permanent shape misfit generated on heating between the near-weld region and the parent structure upon cooling is therefore accommodated to varying degrees within the elastic regime. Because small variations in elastic strain correspond to large variations in stress (owing to the Young's modulus of the metal), numerical solutions appear far more sensitive to the assumed material plasticity theory from a WRS standpoint than they do from a plastic strain standpoint. From this analysis it seems that PEEQ predictions are largely insensitive to the plasticity model chosen, provided cyclic hardening behaviour is accurately captured in the plasticity model.

5.2. Model sensitivity to the assumed material annealing behaviour

Figs. 7(d–f) and 10(a–c) compare longitudinal (σ_{33}) WRS predictions calculated using mixed plasticity theory with different high-temperature annealing assumptions. The results show that changing the annealing assumption has a limited effect on WRS predictions when using mixed plasticity theory. On the other hand, Figs. 8(d–f) and 10(d–f) show that the assumed material annealing behaviour has a significant effect on post-weld plastic strain predictions (PEEQ). Interestingly, the trends observed when varying the material annealing behaviour are opposite those observed when varying the metal plasticity theory. To better understand why significant changes in PEEQ do not necessarily affect predicted WRS, it is useful to examine the evolution of PEEQ after each weld pass; these results are presented in Fig. 11 along the BD line. Considering the evolution of plastic strain under a 1050 °C single-stage annealing assumption as in Fig. 11(a), the strain profile after the first weld pass (PASS.1) indicates a sharp drop in post-weld plastic strain at temperatures exceeding the annealing temperature. This characteristic indicates the amount of metal plasticity accumulated in the annealed material on cooling (~2%) is significantly lower than the plastic strain accumulated on heating (~9%). Similar trends are also observed for single-stage

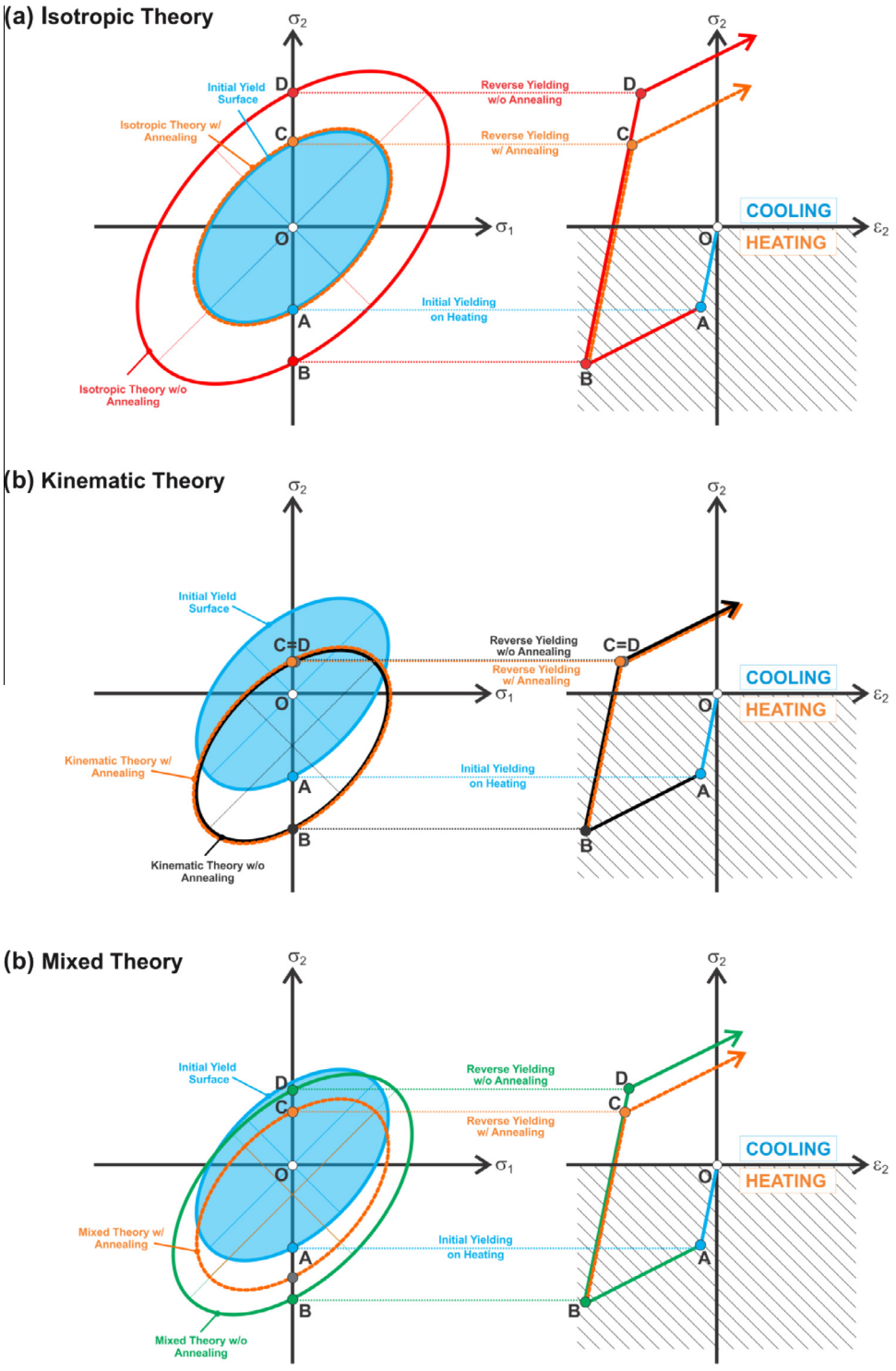

Fig. 12. Schematic highlighting the variation in yield strength between annealed and work-hardened material during welding, using (a) isotropic, (b) kinematic and (c) mixed plasticity theories. Line OAB represents the annealed material response on heating for all models. Line OABD represents the cyclic-hardened material response on heating and subsequent cooling for each plasticity theory, while line OABC represents the annealed material response. Note, for sake of simplification it is assumed (unrealistically) that the unstrained size of the yield surface ($\sigma|_0$) is constant over all temperature ranges.

annealing at 1300°C in Fig. 11(b), and two-stage annealing in Fig. 11(c). Both annealed and work-hardened material will undergo a similar plastic deformation on heating that leads to a shape misfit, and is thus not directly affected by as yet accumulated plastic strain. This strain will indirectly affect WRS predictions however, due to the increase in material yield strength caused by cyclic work hardening. The phenomenon can be shown schematically; a reconstruction of Fig. 2 is presented in Fig. 12 to illustrate the relative behaviour of annealed and work-hardened weld metal under different plasticity theories.

Consider material in the weld HAZ subjected to a representative weld thermal cycle. The following simplifying assumptions are imposed for illustrative purposes: (i) the unstrained size of the yield surface ($\sigma|_0$) is constant over all temperature ranges; (ii)

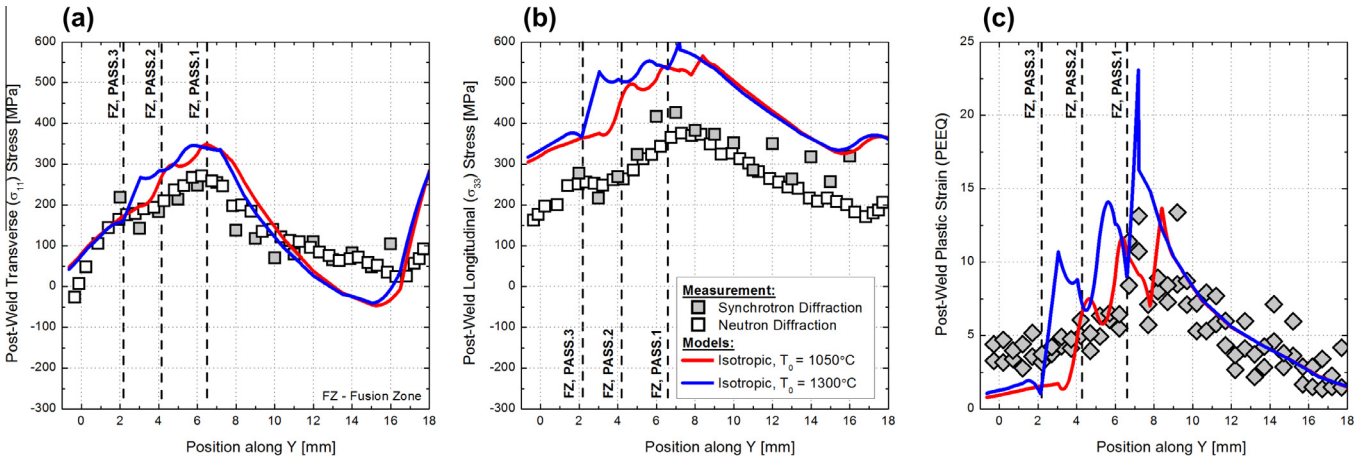

Fig. 13. Model sensitivity to the assumed material annealing behaviour, using isotropic plasticity theory. Variation in (a) the transverse and (b) the longitudinal WRS predictions are presented alongside (c) post-weld plastic strain (PEEQ) predictions, for single-stage annealing temperatures of 1050 °C and 1300 °C.

single-stage annealing occurs at the temperature when perfect plasticity is achieved in the material (when $Q_{inf} = C_i = 0$) and (iii) thermo-mechanical loading is uniaxial (parallel to σ_2 in Fig. 12). As the material is heated during welding, significant transient compressive stresses cause plastic deformation (line OAB in Fig. 12) that leads to a permanent shape misfit between this region and the surrounding undeformed parent structure. The predicted constitutive material response on heating is identical under each plasticity theory (Section 3.1), even though the evolution of the material yield surface differs. The shape misfit formed on heating leads to the development of tensile residual stresses parallel to σ_2 on cooling. Each plasticity theory will predict a different yield strength in tension and thus different WRS (Fig. 7(a–c)), based on how that theory treats cyclic behaviour. Fig. 12 represents typical variations in yield strength as predicted by isotropic, kinematic and mixed plasticity theories.

Should the weld HAZ be heated above the prescribed annealing temperature, two phenomena occur. First, the accumulated plastic strain is eliminated ($\bar{\varepsilon}^{pl}$ = PEEQ = 0). Note that the removal of this plastic flow does not return the material to its original shape; instead a new, undeformed shape is assumed for the material as it must maintain compatibility with the surrounding weldment. Hence, the strain shown after annealing in Fig. 12 indicates the shape change relative to the original material geometry, and not a residual plastic strain. Second, any further accumulation of plastic strain is prevented until the temperature drops below T_0 (i.e. $\dot{\bar{\varepsilon}}^{pl} = 0$). The influence of annealing on the material response upon cooling can be inferred from Eqs. (1) and (2). Removal of $\bar{\varepsilon}^{pl}$ will remove all previous isotropic hardening, causing a contraction of the yield surface back to $\sigma|_0$ and for a fully isotropic plasticity model as in Fig. 12(a), the annealed material will yield at point C upon cooling while the hardened material will yield at point D. For a fully kinematic model as in Fig. 12(b) the annealed material yield surface will retain its size and position in stress space, such that the material will yield upon cooling at the same stress (point C) as the work-hardened material (point D). Consequently, annealing does not influence kinematic hardening behaviour. This insensitivity means that for a mixed hardening model as in Fig. 12(c), the influence of annealing on yield strength will be proportional to the amount of isotropic hardening removed during the anneal. The stress difference between points C and D will be less than for a fully isotropic model and greater than for a kinematic model.

Because the difference between annealed and work-hardened material is greater when using isotropic plasticity theory, WRS predictions made using this theory will be more sensitive to the assumed material annealing behaviour. To prove this fact, Fig. 13 compares predicted WRS and post-weld plastic strain using two different single-stage annealing temperatures (1050 °C and 1300 °C) and isotropic plasticity theory. For both sensitivity analyses using mixed and isotropic plasticity theories, the maximum variation in longitudinal WRS occurs across the 1300 °C isotherm during the last welding pass (Y = 3 mm). This variation is twice as large (120 MPa) when assuming isotropic plasticity as it is when assuming mixed hardening theory (60 MPa), despite the fact that the predicted post-weld plastic strain profiles, shown in Figs. 10(d) and 13(c), are nearly identical. While such variations in WRS are not as large as those observed when varying the plasticity theory (shown in Fig. 9(a) to be 170 MPa at Y = 8.5 mm), it is confirmed that weld models assuming isotropic plasticity theory will be more sensitive to the material annealing behaviour, when predicting both post-weld plastic strain and WRS. *These results therefore suggest that an analyst is more likely to have conservative predictions of both WRS and post-weld plastic strain when using isotropic plasticity theory with a conservative annealing assumption that approaches the melting temperature of the material.*

Similar trends in model sensitivity can be observed when comparing single-stage and two-stage annealing assumptions. Fig. 10(d) shows that the post-weld plastic strain predicted using two-stage annealing behaviour lies somewhere between the two different single-stage annealing results, while Fig. 10(a) shows how this trend corresponds to a predicted WRS profile that also lies between the single-stage annealing results. The clear advantage of using a two-stage annealing assumption is that it gives the analyst more flexibility when defining the cyclic thermo-mechanical hardening behaviour of welding processes. As previously discussed by Smith et al. (2012a), two-stage annealing will also eliminate sharp discontinuities in PEEQ, which are not representative of the actual material response. While the upper annealing temperature T_2 is identical to the single-stage T_0 of 1300 °C, significantly less PEEQ is accumulated (e.g. at Y = 3 mm) due to the lack of isotropic hardening at temperatures above T_1 (800 °C), as shown in Fig. 11(c). While such information can significantly affect model accuracy when predicting post-weld plastic strain, a two-stage annealing assumption requires the necessary empirical data to define T_1 and T_2.

6. Conclusions

An assessment of weld model sensitivity to the assumed constitutive material behaviour has been conducted using a validated FE model for a three-pass slot weld in austenitic steel. Model sensitivity to two key material assumptions was assessed: (i) the assumed

material plasticity theory and (ii) the assumed material annealing behaviour. The sensitivity was quantified using both weld residual stresses (WRS) and post-weld plastic strain (PEEQ) predictions. The following conclusions were drawn:

1. In general, model predictions of WRS and PEEQ are in good agreement with measurement, however variations between measured and predicted data exist in the weld metal. Inaccurate WRS predictions arise in the weld metal due to improper specification of the weld metal yield strength in the FE model. Measurement inaccuracies in post-weld plastic strain are related to the indirect hardness method used to measure plastic strain. While this measurement technique accurately captures accumulated plastic strain in the parent metal, the technique fails to account for significant microstructural differences in the weld and HAZ, which render the trends generated for the parent metal inapplicable in these regions.
2. An examination of model sensitivity to the assumed material plasticity theory reveals the choice of theory will have a significant influence on the predicted WRS, but not the post-weld plastic strain. This result is believed to occur since each plasticity model will predict slightly different elastic behaviour to accommodate the shape misfit between the weld region and remainder of the parent metal on cooling. As slight changes to the amount of accumulated elastic strain will result in large changes to the internal stress, this relative sensitivity (between WRS and PEEQ) is justified.
3. An examination of model sensitivity to the assumed material annealing behaviour reveals this sensitivity is dependent on the plasticity theory used. It is observed that most of the post-weld plastic strain is accumulated during heating, where compressive stresses in the near-weld region generate plastic flow. Post-weld plastic strain predictions are thus highly sensitive to annealing assumptions, since annealing will remove this initial plastic strain. Prior strain hardening is shown to have a variable influence on WRS predictions; a weak influence is observed when isotropic hardening is offset by Bauschinger effects (i.e. mixed plasticity theory), while a strong influence is observed when Bauschinger effects are not considered (i.e. isotropic plasticity theory). The influence is therefore a function of the amount of isotropic hardening present in the material; however, WRS predictions are less sensitive to annealing behaviour than they are to the plasticity theory used, in all cases.
4. It is shown that the mixed plasticity theory in combination with a two-stage annealing approximation gives the most realistic prediction of both WRS and post-weld plastic strain. It is, however, acknowledged that obtaining the experimental data for the mixed plasticity theory and proper calibration of two-stage annealing temperatures might be difficult. Therefore, it is recommended that the analyst seeking conservative predictions of both peak tensile WRS and post-weld plastic strain use an isotropic plasticity theory with a conservative single-stage annealing temperature (i.e. one that approaches the melting temperature of the parent metal).

Acknowledgments

The authors gratefully acknowledge the assistance of Dr. P. Dayal (ANSTO) with cross-weld hardness measurements, ECHIDNA high-resolution powder diffraction measurements by Dr. M. Abdeev (ANSTO) and work by Dr. N. Ben Moussa (L'École Supérieure des Sciences et Techniques de Tunis) on the correlation between plastic strain and micro-hardness. All previous residual stress measurements and predictions under the auspices of the European Network on Neutron Techniques Standardisation for Structural Integrity (NeT) programme, Task Group 4 are also acknowledged.

References

ABAQUS, 2007. A Novel Approach to Annealing using ABAQUS – Behaviour with Soft Annealing. SIMULIA.
Ben Moussa, N., 2013. Optimisation des performances des surfaces usinées par le contrôle des paramètres des procédés: Approches expérimentale et numérique. Ecole Supérieure des Sciences et Techniques de Tunis, vol. Mécanique. Tunis: Ecole Supérieure des Sciences et Techniques de Tunis.
Brule, A., Kirstein, O., 1040. Physica B, 385–386, Part 2: 1040.
Dewees, D.J., Prueter, P.E., Kummari, S.R., 2014. American Society of Mechanical Engineers. Pressure Vessels and Piping Division (Publication), PVP.
Hutchings, M.T., Withers, P.J., Holden, T.M., Lorentzen, T., 2005. Introduction to the Characterization of Residual Stress by Neutron Diffraction. CRC Press.
Liss, K.-D., Hunter, B., Hagen, M., Noakes, T., Kennedy, S., 1010. Physica B, 385–386, Part 2: 1010.
Martins, R.V., 2009. NeT – Task Group 4: Three-Pass Slot Weld Specimen in Austenitic Stainless Steel. Protocol for the Destructive and Non-Destructive Determination of Residual Stress in Three-Pass Slot Weld Specimens in Austenitic Stainless Steel.
Martins, R.V., Ohms, C., Decroos, K., 2010. Mater. Sci. Eng. A 527, 4779.
Muránsky, O., Smith, M.C., Bendeich, P.J., Holden, T.M., Luzin, V., Martins, R.V., Edwards, L., 2012a. Int. J. Solids Struct. 49, 1045.
Muránsky, O., Hamelin, C.J., Smith, M.C., Bendeich, P.J., Edwards, L., 2012b. Comput. Mater. Sci. 54, 125.
Muránsky, O., Smith, M.C., Bendeich, P.J., Hosseinzadeh, F., Edwards, L., 2014. Eng. Fract. Mech. 126, 40.
Shchaeffler, A.L., 1949. Met. Prog. 56.
SIMULIA, 2014. ABAQUS/Standard. Dassault Systems.
Smith, M.C., 2006. Development of mixed isotropic-kinematic material hardening models for finite element simulation of austenitic steel welds. E/REP/BDBB/0092/AGR/06, Revision 000: British Energy.
Smith, R.M., 2010. FEAT-WMT: Weld-Modelling Tool User Guide. FEAT-WMT: Weld-Modelling Tool User Guide: FeatPlus Limited.
Smith, M.C., Smith, A.C., Nadri, B., Bendeich, P.J., Carr, D.G., 2009. Optimisation of mixed hardening material constitutive models for weld residual stress simulation using the NeT Task Group 1 single bead-on-plate benchmark problem. In: ASME Pressure Vessels and Piping Conference, vol. 6. Prague, Czech Republic, p. 303.
Smith, M.C., Bouchard, P.J., Turski, M., Edwards, L., Dennis, R.J., 2012a. Comput. Mater. Sci. 54, 312.
Smith, M.C., Muránsky, O., Austin, C., Bendeich, P.J., Edwards, L., 2012b. Optimised modelling of weld metal constitutive behaviour in the NeT TG4 international weld simulation and measurement benchmark, In: 2012 ASME Pressure Vessels & Piping Conference Toronto, Canada.
Turski, M., Smith, M.C., Bouchard, P.J., Edwards, L., Withers, P.J., 2009. J. Press. Vessel Technol. 131, 1.
Withers, P.J., 2001a. Bhadeshia HKDH. Mater. Sci. Technol. 17, 366.
Withers, P.J., 2001b. Bhadeshia HKDH. Mater. Sci. Technol. 17, 355.
Withers, P.J., 2007. Rep. Progr. Phys. 70, 2211.